

# The Twin Paradox in Quantum Field Theory

Matheus H. Zambianco<sup>1,2,3,\*</sup> and T. Rick Perche<sup>4,†</sup>

<sup>1</sup>*Department of Applied Mathematics, University of Waterloo, Waterloo, Ontario, N2L 3G1, Canada*

<sup>2</sup>*Perimeter Institute for Theoretical Physics, Waterloo, Ontario, N2L 2Y5, Canada*

<sup>3</sup>*Institute for Quantum Computing, University of Waterloo, Waterloo, Ontario, N2L 3G1, Canada*

<sup>4</sup>*Nordita, KTH Royal Institute of Technology and Stockholm University,  
Hannes Alfvéns väg 12, 23, SE-106 91 Stockholm, Sweden*

Vacuum fluctuations in quantum field theory impose fundamental limitations on our ability to measure time in short scales. To investigate the impact of universal quantum field theory effects on observer-dependent time measurements, we introduce a clock model based on the vacuum decay probability of a finite-sized quantum system. Using this model, we study a microscopic twin paradox scenario and find that, in the smallest scales, time is not only dependent on the trajectory connecting two events, but also on how vacuum fluctuations interact with the microscopic details of the clocks.

## I. INTRODUCTION

Relativity predicts that the passage of time is relative: two clocks may yield two different measurements of time between the same two events, depending on their trajectory in spacetime. Perhaps the most clear example of the relativity of the passage of time is illustrated in the *twin paradox* [1–4], where two twins follow different worldlines—one twin remains on Earth, whereas the other travels aboard a spacecraft. Upon reunion, they find that the traveling twin ages less. The apparent paradox arises from the incorrect assumption that the twins’ kinematics are symmetric, when, in fact, only one twin accelerates throughout their motion. The age difference is a consequence of the fact that inertial trajectories locally maximize proper time between events.

Although the relative passage of time has been verified by experiments [5–9], the classical relativistic description is not expected to hold in arbitrarily small scales. Indeed, quantum theory imposes fundamental restrictions on the precision of space and time measurements [10, 11]. Moreover, there is no universal representation for a time observable within quantum mechanics [12–14]. Instead, time is more precisely investigated through the physical realization of clocks: systems whose dynamics can be used to parametrize the occurrence of physical events, enabling an operational measurement of elapsed time [15–17]. Indeed, the most precise measurements of time intervals are realized by atomic clocks [18–20], which can measure times of the order of  $10^{-18}$  s [21, 22].

In this manuscript, we are concerned with the observer-dependent passage of time in scales where the notion of ideal clocks from classical relativity cannot be implemented, which we study through a microscopic twin paradox scenario. Although a quantum version of the twin paradox with clocks in superposition was explored in [23], here we focus on the standard twin paradox scenario in scales where universal quantum field theory

(QFT) effects become relevant for tracking the passage of time. Indeed, QFT yields the most accurate predictions for relativistic effects in quantum physics. It becomes particularly relevant for the description of non-inertial systems, such as in the Unruh effect [24–27] and short time effects [28–31]. Thus, a complete study of the relativity of time at the smallest scales must take QFT into account.

Indeed, it is precisely in time-scales comparable to the system’s light crossing time that the vacuum fluctuations of quantum fields plays more significant roles [31]. As we will see, in a microscopic twin-paradox scenario where the clock’s size is non-negligible compared to the measured times, parameters that are usually irrelevant for time measurements, such as the clock’s shape and specific internal dynamics, end up playing crucial roles.

## II. NON-PERIODIC CLOCKS

The most precise clocks available today utilize the oscillation between two quantum states of atoms to define a frequency standard [18]. In these atomic clocks, the typical scenario involves the preparation of the atoms in an equilibrium state with precisely tuned electromagnetic radiation that promotes periodic de-excitations, while also repopulating the atom’s excited state. Counting the emitted photons when the atoms deexcite directly gives a count of the elapsed time, analogous to “ticks” of a clock. Nonetheless, atomic clocks are not naturally suited to compare short times measured by observers that undergo different trajectories between two events, such as in a twin paradox scenario. For instance, identifying the events where two atomic clocks coincide would by itself disrupt their periodic dynamics, which requires relatively long times to be reestablished [22]. Furthermore, atomic clocks are significantly affected by drastic accelerations [32], hindering their application to explore relativistic effects.

To account for highly non-equilibrium situations and relativistic motion in time scales comparable to the light-crossing time of the clocks, we propose a different clock

\* mhzambianco@uwaterloo.ca

† rick.perche@su.se

model. We consider an hourglass-type clock, in which a non-periodic physical process is used to keep track of time between events. For instance, a non-periodic process that can be used to track time is carbon dating. The decay rate of  $^{14}\text{C}$  to  $^{12}\text{C}$  is  $\mathcal{F} \approx 3.84 \times 10^{-12} \text{s}^{-1}$  (corresponding to a half-life of 5730 years). Although this process is typically used to estimate times of scales comparable to its half-life, it is possible to adapt it to measure times of the order of seconds. As an example, if one possesses  $N = 10^{15}$  Carbon-14 atoms, it is expected that each second,  $N_d \approx N\mathcal{F} \times 1\text{s} \approx 3840$  atoms will decay. Assuming that one can precisely count the number of  $^{14}\text{C}$  atoms in a sample, one can use this number to measure times of the order of fractions of seconds.

More generally, in a decay process from a state  $|e\rangle$  (excited) to a state  $|g\rangle$  (ground), the rate of change of the probability of finding the system in its excited state is typically proportional to itself,  $dP_e = -\mathcal{F}P_e(t)dt$ , and the probability of remaining in the excited state is exponentially decreasing with time. If the system starts in the state  $|e\rangle$ ,  $P_e(t) = e^{-\mathcal{F}t}$ , with  $\mathcal{F}$  the decay rate of the system. If  $|g\rangle$  and  $|e\rangle$  are the only states under consideration, we then have  $P_g(t) = 1 - e^{-\mathcal{F}t}$  for the probability of the system transitioning into the state  $|g\rangle$ . If  $\mathcal{F}$  is such that  $\mathcal{F}t \ll 1$ , we then have  $P_g(t) \approx \mathcal{F}t$ , in which case the decay probability can be directly used to track time. Moreover, a process of this type is particularly robust against disruptions and measurements.

This clock model operates as an hourglass in the following sense: when interacting with the vacuum of a quantum field, any quantum system prepared in its excited state  $|e\rangle$  will tend to become deexcited, slowly changing its state to  $|g\rangle$  if enough time elapses, at a rate that is proportional to the classical proper time of its trajectory. The analogy is that while the clock is in the state  $|e\rangle$  “all of the sand is at the top”, whereas the final state  $|g\rangle$  corresponds to “all the sand at the bottom”.

### III. NON-PERIODIC CLOCKS IN QFT

To fully take into account QFT effects within our model, we consider a (small) finite-sized quantum system undergoing a trajectory  $\mathbf{z}(\tau)$ , prepared in its excited state  $|e\rangle$ . We switch on its interaction with the vacuum of an external, free quantum field at a certain event  $\mathbf{x}_i$ , at the center of the localized system. We then switch off the interaction at a later event  $\mathbf{x}_f$ , also located at the center of the clock. Its de-excitation probability to a ground state  $|g\rangle$  at the end of the interaction is proportional to the interaction time, and can be used to measure the time elapsed between the events  $\mathbf{x}_i$  and  $\mathbf{x}_f$ , as defined by an observer undergoing  $\mathbf{z}(\tau)$ .

To leading order in the coupling parameter of the interaction ( $\lambda$ ), the de-excitation probability of this localized system depends only on a few parameters that determine the interaction, such as the shape and spacetime trajectory [33–35] of the clock, as well as the energy gap  $\Omega$

between the states  $|g\rangle$  and  $|e\rangle$ . In the hourglass analogy, these parameters define how fast the sand is allowed to fall. Concretely, when the clock is linearly coupled to an external real scalar field, its de-excitation probability (to leading order in  $\lambda$ ), can be written as

$$P_D = \lambda^2 \int dV dV' \Lambda(\mathbf{x}) \Lambda(\mathbf{x}') e^{i\Omega(\tau(\mathbf{x}) - \tau(\mathbf{x}'))} W(\mathbf{x}, \mathbf{x}'), \quad (1)$$

where  $\tau(\mathbf{x})$  is a local extension of the clock’s proper time around the trajectory  $\mathbf{z}(\tau)$  [33, 35–37],  $dV = \sqrt{-g} d^4\mathbf{x}$  is the invariant spacetime volume element,  $W(\mathbf{x}, \mathbf{x}')$  is the vacuum two-point function of the external free quantum field, and  $\Lambda(\mathbf{x})$  determines the clock’s spatial profile and the switch on and off of the interaction. In particular, a rigid clock localized around the trajectory  $\mathbf{z}(\tau)$  with comoving (Fermi normal [38]) coordinates  $(\tau, \boldsymbol{\xi})$  [35, 37, 39] is such that

$$\Lambda(\mathbf{x}) = F(\boldsymbol{\xi}) \mathbb{1}_{[\tau_i, \tau_f]}(\tau) \quad (2)$$

for  $\tau \in [\tau_i, \tau_f]$ , where the clock tracks elapsed time between the events  $\mathbf{z}(\tau_i) = \mathbf{x}_i$  and  $\mathbf{z}(\tau_f) = \mathbf{x}_f$ . The function  $F(\boldsymbol{\xi})$  is determined by the relevant spatial profile of the interaction between the clock and field, usually given by the wavefunctions of the states  $|g\rangle$  and  $|e\rangle$  [37, 40–43]. Furthermore, this behaviour is universal to localized systems interacting with an external field, present in short-time light-matter interactions [43–45], the interactions of fermions and neutrinos [46, 47], as well as larger-scale systems, such as lasers interacting with Bose-Einstein condensates [48]. For instance, in the case of an atom interacting with an external electromagnetic field,  $F(\boldsymbol{\xi})$  would be a function of the electron orbitals and  $W(\mathbf{x}, \mathbf{x}')$  would be replaced by the two-point function of the electromagnetic field [43–45].

When the clock’s size (as effectively described by the function  $F(\boldsymbol{\xi})$ ) is negligible compared to the interaction times, clocks that operate according to Eqs.(1) and (2) effectively behave as ideal clocks. Indeed, since Eq. (1) is also the leading order de-excitation probability of an Unruh-DeWitt detector [24, 40, 49] interacting with a scalar field, the de-excitation rate obtained through the limit

$$\mathcal{F} \equiv \lim_{\Delta\tau \rightarrow \infty} \frac{P_D}{\Delta\tau} \quad (3)$$

is finite (see e.g. [50] for stationary examples). Moreover, it depends only on the clock’s energy gap  $\Omega$ , in its spatial profile  $F(\boldsymbol{\xi})$ , and potentially on its trajectory in spacetime through the comoving coordinates  $(\tau, \boldsymbol{\xi})$ . This implies that in this long-time regime, the leading order de-excitation probability is proportional to the elapsed proper time  $\Delta\tau$ , thus behaving like an ideal clock. In Appendix B we also show that, for inertial clocks in Minkowski spacetime, the approximation  $P_D \approx \mathcal{F}\Delta\tau$  becomes valid for relatively short times compared to the clock’s light-crossing time and energy gap. For instance,

when  $\Delta\tau$  is larger than 30 times its light-crossing time, the relative deviation  $|P_D - \mathcal{F}\Delta\tau|/\mathcal{F}\Delta\tau$  remains smaller than 2%, with the difference being due to universal finite-time QFT effects. We can then define the proper time tracked by the clock between the events  $\mathbf{x}_i$  and  $\mathbf{x}_f$  as  $\Delta\tau_D \equiv P_D/\mathcal{F}^1$ . A clock is then defined by its energy gap  $\Omega$  and proper spatial profile encoded in the function  $F(\boldsymbol{\xi})$ . However, clocks with the same proper shape and proper energy gap may still behave differently due to local and non-inertial QFT effects due to how they sample the two-point function in Eq. (1).

Finally, observe that any operational definition of time must take into account universal vacuum effects in QFT due to local couplings and non-inertial motion (such as vacuum fluctuations and the Unruh effect [24, 25, 27, 40]), and the clock model presented here has the advantage of naturally incorporating these effects. For instance, it is fundamental that our clocks have a finite size; otherwise, UV correlations of QFT would result in a divergent leading-order de-excitation probability [33].

#### IV. TWIN PARADOX IN QFT

We consider a twin paradox scenario by modeling the internal dynamics of clocks fully within QFT, as above. We will see that in the limit of sufficiently long times, these clocks yield the standard predictions of relativity. However, for time scales that are a few orders of magnitude larger than the clocks' proper size, we find corrections due to QFT effects.

The twin paradox is usually formulated in terms of two twins, Alice and Bob, who undergo different trajectories connecting two events  $\mathbf{x}_i$  and  $\mathbf{x}_f$ , where Alice remains inertial throughout her motion and Bob experiences acceleration. When they reunite and compare clocks, they conclude that Alice has aged more than Bob. The description of the standard setup assumes both Alice and Bob carry an ideal pointlike clock, which tracks the proper time along their trajectories and can be used to compare how much they have aged.

If, instead, one wishes to consider more realistic finite-sized clocks, one has to be careful about how to compare the twins' motion at the initial and final events. Indeed, observers moving relative to one another have different rest spaces, and even clocks with the same shape would start their trajectory at different times within their spatial extension. Thus, when using extended clocks, it is

crucial that both twins start and end their motion at rest with respect to each other. We then consider Alice undergoing the trajectory  $\mathbf{z}_A(t) = (t, 0, 0, 0)$  parameterized by her (inertial) proper time  $t$  and Bob following the trajectory  $\mathbf{z}_B(\tau) = (t(\tau), x(\tau), 0, 0)$  parameterized by the (non-inertial) proper time  $\tau$ . His trajectory starts inertial and constantly accelerates with proper acceleration  $a$  in the  $x$  direction for  $\tau \in (0, T/4)$ , followed by a portion with constant acceleration  $-a$  for  $\tau \in (T/4, 3T/4)$ , and another trajectory with constant acceleration  $a$  for the final part,  $\tau \in (3T/4, T)$  ending at rest with respect to Alice and meeting her again at  $\tau = T$  (see Appendix A for the explicit expressions of  $t(\tau)$  and  $x(\tau)$ ). With these choices, the trajectories are initially comoving, starting their motion at the event  $\mathbf{x}_i = (0, \mathbf{0})$  in inertial  $(t, \mathbf{x})$  coordinates. The twins meet again at the event  $\mathbf{x}_f = (T_A, 0)$  with

$$T_A = \frac{4}{a} \sinh\left(\frac{aT}{4}\right), \quad (4)$$

where the trajectories are comoving once again. When they meet, a classical ideal clock carried by Alice would indicate an elapsed proper time of  $T_A^2$  between events  $\mathbf{x}_i$  and  $\mathbf{x}_f$ , whereas the proper time measured by Bob between these events would be  $T_B = T$ .

To study the different passage of time for microscopic observers in QFT, we consider two twins, Alice and Bob undergoing the trajectories  $\mathbf{z}_A(t)$  and  $\mathbf{z}_B(\tau)$  carrying identical clocks, as described in the previous section. The clocks are then finite-sized quantum systems with the same energy gap  $\Omega$  and proper spatial profile defined by

$$F(\mathbf{u}) = \frac{e^{-\|\mathbf{u}\|^2/2\sigma^2}}{(\sqrt{2\pi}\sigma)^3}, \quad (5)$$

where  $\|\mathbf{u}\|^2 = \delta_{ij}u^i u^j$ . With the choice above,  $\sigma$  controls the spatial extension of the clock, also corresponding to their light-crossing time in units where  $c = 1$ . Explicitly, the de-excitation probability of each clock can be written as in Eq. (1) with spacetime smearings  $\Lambda_A(\mathbf{x})$  and  $\Lambda_B(\mathbf{x})$  given by

$$\Lambda_A(t, \mathbf{x}) = \mathbb{1}_{[0, T_A]}(t) F(\mathbf{x}), \quad (6)$$

$$\Lambda_B(\tau, \boldsymbol{\xi}) = \mathbb{1}_{[0, T_B]}(\tau) F(\boldsymbol{\xi}), \quad (7)$$

in their respective Fermi normal coordinates. Notice that while Alice's Fermi normal coordinates are simply  $(t, \mathbf{x})$ , Bob's coordinates  $(\tau, \boldsymbol{\xi})$  are constructed from comoving coordinates for each uniformly accelerated portion of its trajectory. The explicit coordinate transformations are given in Appendix A, and the coordinate lines in the  $(t, \mathbf{x})$

<sup>1</sup> Notice that it is not possible to directly access the excitation probability using a single clock through a one-shot experiment. Instead, one should repeat the experiment  $N$  times under the exact same circumstances. Then, if the clock decays in  $N_d$  of those experiments, the elapsed time between events  $\mathbf{x}_i$  and  $\mathbf{x}_f$  as measured by this clock model is given by  $\Delta\tau \equiv \mathcal{F}^{-1}N_d/N \approx P_D/\mathcal{F}$ .

<sup>2</sup> Notice that  $T_A$  ends up depending on  $a$  and  $T$ , as it corresponds to the proper time at which Bob meets Alice, and Bob's trajectory is determined by these parameters. Overall,  $T_A$  and  $T_B$  are related by  $T_B = \frac{4}{a} \sinh^{-1}(aT_A/4)$ .

plane are depicted in Fig. 1.

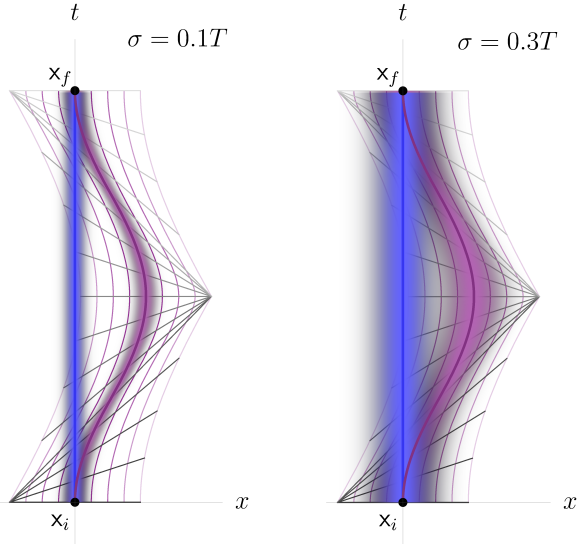


Figure 1. Density plot of the regions of interaction of Alice (blue) and Bob (purple) for  $\sigma = 0.1T$  and  $\sigma = 0.3T$ . The rest surfaces of constant  $\tau$  are shown in gray, and the curves of constant  $\xi$  are shown in purple.

We can analyze the effects of QFT on the twin paradox by comparing the classical ratio of proper times

$$\frac{T_B}{T_A} = \frac{aT}{4 \sinh(\frac{aT}{4})} \quad (8)$$

with the ratio of the times measured by the quantum clocks carried along the respective trajectories, given by  $P_B/P_A$ .

## V. RESULTS

Using the setup above, we numerically evaluate the de-excitation probabilities  $P_A$  and  $P_B$  for Alice's and Bob's clocks, respectively. Details of the expressions used in these calculations are given in Appendix A. We then compare the ratio of the clock's elapsed times,  $P_B/P_A$ , for different clock sizes and different trajectories. Observe that by fixing the value of the product  $aT$ , we select trajectories for which the classical proper time  $T_B/T_A$  remains constant (as in Eq. (8)), allowing a fair comparison between different cases. Figure 2 displays  $P_B/P_A$  for multiple clock sizes with energy gap  $\Omega = 2T_0$  as a function of  $T/T_0$  for a fixed timescale  $T_0$  when  $aT = 2$  and  $aT = 4$ . In Appendix B we show that for the parameters used in Fig. 2, Alice's inertial clock effectively agrees with the times predicted by relativity (e.g. accuracy of  $\sim 1\%$  for  $\sigma = 0.1T_0$ ).

Notice that in the long time regime (with constant  $aT$ ), the predictions provided by the quantum clocks agree with the classical ratio. This is no surprise, as keeping the ratio of proper times constant and considering

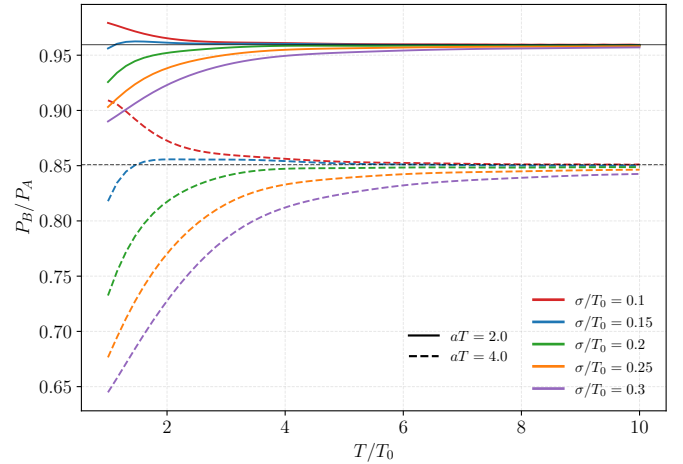


Figure 2. Ratio between Bob's elapsed time and Alice's elapsed time for different clock sizes (controlled by the parameter  $\sigma$ ), with energy gap  $\Omega = 2T_0$ , and for trajectories satisfying  $aT = 2$  and  $aT = 4$ .

$T \rightarrow \infty$  implies  $a \rightarrow 0$ , in which case the rates  $\mathcal{F}_B$  and  $\mathcal{F}_A$  match exactly and the de-excitation probabilities behave as  $P_B \approx \mathcal{F} T_B$  and  $P_A \approx \mathcal{F} T_A$ , with the same de-excitation rate  $\mathcal{F}$ . Notice that even in this limit the trajectories are still within the relativistic regime, as the maximum velocity reached by Bob relative to Alice is  $v = \tanh(\frac{aT}{4})$  ( $v \approx 0.46c$  and  $v \approx 0.76c$  for  $aT = 2$  and  $aT = 4$ , respectively).

Nonetheless, in the regime where the clock's light-crossing time  $\sigma$  is not negligible compared to  $T$ , deviations appear compared to the predictions of classical relativity. We observe that they (i) grow with clock size, since larger clocks sample field degrees of freedom further away from the central trajectory, and (ii) increase with the acceleration  $a$ , a manifestation of non-inertial QFT effects. This aligns with prior works showing that QFT features dominate at short times [31, 51].

## VI. COMPARISON WITH ATOMIC CLOCKS

In the regime of short interaction times, the value of  $P_B/P_A$  yields QFT corrections to measurements of time. Moreover, when one considers specific physical systems, the time scales where those effects are relevant turn out to be within current atomic clock precision. Indeed, a single-atom atomic clock (see, e.g., [22]), has a size of the order of  $\sigma \sim 10^{-10}\text{m}$ , and in Fig. 2, we see that QFT corrections are relevant when the interaction time  $T$  is of the order (reintroducing the speed of light  $c$ )

$$T \sim 10 \frac{\sigma}{c}. \quad (9)$$

As mentioned before, the best atomic clocks currently available can measure times of the order of  $10^{-18}\text{ s}$  [21,

22]. The characteristic time over which deviations from the classical result become observable is then of the order of  $T \sim 10^{-17}$  s, which is well within the precision of current atomic clocks. However, for this effect to be observed, atomic clocks would have to be accelerated and decelerated to at least 45% of the speed of light within times of the order of attoseconds.

Moreover, as we discussed earlier, the current setup of atomic clocks is not suitable for measuring times associated with observers undergoing trajectories for arbitrarily short durations, significantly disturbing their periodic behaviour. Also, in experiments where atomic clocks are used to probe observed-dependent time dilation [52, 53], the acceleration (and gravitational fields) involved are much smaller than the scales where the effects discussed here are relevant. Indeed, utilizing atomic clocks to measure times of the order of  $T \sim 10^{-17}$  s, the values used in Fig. 2 would correspond to accelerations of the order of  $a \sim 10^{25}$  m/s<sup>2</sup>, which have not yet been experimentally tested.<sup>3</sup>

In comparing our clock model with standard atomic clocks, it is also important to recall that single-atom atomic clocks usually employ a trapped ion (or neutral atom), confined by oscillatory electromagnetic fields and laser-cooled [18]. Beyond natural challenges in subjecting this setup to relativistic accelerations, the preparation of atomic clocks requires smooth Rabi pulses (to measure the current quantum state of the atom) that last typically hundreds of milliseconds [22]. For these time scales, our model predicts that short-time corrections are strongly suppressed, and the clock exhibits essentially classical relativistic behavior.

## VII. CONCLUSIONS

Time, as a physical observable, should be defined operationally by physical systems, not as a parameter of a classical theory. Although atomic clocks are the state of the art in time measurements, they require sustainable periodic processes, being unsuitable for describing the observer dependence of time for trajectories that reach significant fractions of the speed of light within few clock ticks. Furthermore, in the shortest time scales, non-

equilibrium processes are ubiquitously affected by universal local effects of QFT. To accurately describe these effects in a twin-paradox scenario, we introduced a clock model that incorporates fundamental QFT effects, tracking time through its decay probability. While this clock reproduces standard relativistic time dilation in the long-time regime, it also exhibits deviations at short interaction times due to vacuum fluctuations in finite spacetime regions.

While quantum mechanics imposes fundamental limitations to the precision of time measurements due to uncertainty relations [54, 55], when taking the step into QFT, the limitations become even more drastic. Times tracked become explicitly dependent on the microscopic properties of the clock: clocks with different shapes and different internal dynamics probe vacuum fluctuations differently, directly affecting the time tracked by them. Our results show that on microscopic scales, two distinct observers following the same trajectory between the same two events will, in general, experience different notions of time. In scales where universal QFT effects are relevant, time is not only dependent on the trajectory, but also on the specific microscopic details of the physical systems used to track it.

## ACKNOWLEDGMENTS

MHZ thanks Profs. Achim Kempf and Eduardo Martín-Martínez for supervision, and Prof. Achim Kempf for his funding through the Dieter Schwarz grant. TRP is thankful for financial support from the Olle Engkvist Foundation (no.225-0062). Research at Perimeter Institute is supported in part by the Government of Canada through the Department of Innovation, Science and Industry Canada and by the Province of Ontario through the Ministry of Colleges and Universities. Perimeter Institute and the University of Waterloo are situated on the Haldimand Tract, land that was promised to the Haudenosaunee of the Six Nations of the Grand River, and is within the territory of the Neutral, Anishinaabe, and Haudenosaunee people. Nordita is partially supported by Nordforsk.

- 
- [1] E. F. Taylor, *Spacetime Physics*, edited by J. A. Wheeler (W. H. Freeman, San Francisco, 1966).
  - [2] J. D. Barrow and J. Levin, Twin paradox in compact spaces, *Phys. Rev. A* **63**, 044104 (2001).
  - [3] F. L. Markley, Relativity twins in the kerr metric, *American Journal of Physics* **41**, 1246 (1973).

<sup>3</sup> Notice that although the Unruh effect would be visible for these accelerations, the short-time duration where the local QFT effects are relevant prevents any significant thermalization effects.

- [4] L. M. Sokolowski, On the twin paradox in static spacetimes: I. schwarzschild metric, *General Relativity and Gravitation* **44**, 1267 (2012).
- [5] B. Rossi and D. B. Hall, Variation of the rate of decay of mesotrons with momentum, *Phys. Rev.* **59**, 223 (1941).
- [6] J. C. Hafele and R. E. Keating, Around-the-world atomic clocks: Predicted relativistic time gains, *Science* **177**, 166 (1972).
- [7] B. Botermann, D. Bing, C. Geppert, G. Gwinner, T. W. Hänsch, G. Huber, S. Karpuk, A. Krieger, T. Kühl, W. Nörtershäuser, C. Novotny, S. Reinhardt, R. Sánchez,

- D. Schwalm, T. Stöhlker, A. Wolf, and G. Saathoff, Test of time dilation using stored  $\text{Li}^+$  ions as clocks at relativistic speed, *Phys. Rev. Lett.* **113**, 120405 (2014).
- [8] C. W. Chou, D. B. Hume, T. Rosenband, and D. J. Wineland, Optical clocks and relativity, *Science* **329**, 1630 (2010).
- [9] P. Delva, J. Lodewyck, S. Bilicki, E. Bookjans, G. Vallet, R. Le Targat, P.-E. Pottie, C. Guerlin, F. Meynadier, C. Le Poncin-Lafitte, O. Lopez, A. Amy-Klein, W.-K. Lee, N. Quintin, C. Lisdar, A. Al-Masoudi, S. Dörscher, C. Grebing, G. Grosche, A. Kuhl, S. Raupach, U. Sterr, I. R. Hill, R. Hobson, W. Bowden, J. Kronjäger, G. Marra, A. Rolland, F. N. Baynes, H. S. Margolis, and P. Gill, Test of special relativity using a fiber network of optical clocks, *Phys. Rev. Lett.* **118**, 221102 (2017).
- [10] H. Salecker and E. P. Wigner, Quantum limitations of the measurement of space-time distances, *Phys. Rev.* **109**, 571 (1958).
- [11] Y. J. NG and H. van DAM, Limitation to quantum measurements of space-time distances, *Annals of the New York Academy of Sciences* **755**, 579–584 (1995).
- [12] W. Pauli, *General Principles of Quantum Mechanics* (Springer-Verlag, Berlin, 1980).
- [13] W. G. Unruh and R. M. Wald, Time and the interpretation of canonical quantum gravity, *Physical Review D* **40**, 2598 (1989).
- [14] J. G. Muga, R. Sala Mayato, and I. L. Egusquiza, eds., *Time in Quantum Mechanics*, 2nd ed., Lecture Notes in Physics, Vol. 734 (Springer-Verlag, Berlin Heidelberg, 2008).
- [15] P. Erker, M. T. Mitchison, R. Silva, M. P. Woods, N. Brunner, and M. Huber, Autonomous quantum clocks: Does thermodynamics limit our ability to measure time?, *Phys. Rev. X* **7**, 031022 (2017).
- [16] X. He, P. Pakkiam, A. A. Gangat, M. J. Kewming, G. J. Milburn, and A. Fedorov, Effect of measurement back-action on quantum clock precision studied with a superconducting circuit, *Phys. Rev. Appl.* **20**, 034038 (2023).
- [17] A. R. H. Smith and M. Ahmadi, Quantum clocks observe classical and quantum time dilation, *Nature Communications* **11**, 5360 (2020).
- [18] A. D. Ludlow, M. M. Boyd, J. Ye, E. Peik, and P. O. Schmidt, Optical atomic clocks, *Rev. Mod. Phys.* **87**, 637 (2015).
- [19] T. L. Nicholson, S. L. Campbell, R. B. Hutson, G. E. Marti, B. J. Bloom, R. L. McNally, W. Zhang, M. D. Barrett, M. S. Safronova, G. F. Strouse, W. L. Tew, and J. Ye, Systematic evaluation of an atomic clock at  $2 \times 10^{-18}$  total uncertainty, *Nature Communications* **6**, 6896 (2015).
- [20] W. F. McGrew, X. Zhang, R. J. Fasano, S. A. Schäffer, K. Beloy, D. Nicolodi, R. C. Brown, N. Hinkley, G. Milani, M. Schioppa, T. H. Yoon, and A. D. Ludlow, Atomic clock performance enabling geodesy below the centimetre level, *Nature* **564**, 87 (2018).
- [21] E. Oelker, R. B. Hutson, C. J. Kennedy, L. Sonderhouse, T. Bothwell, A. Goban, D. Kedar, C. Sanner, J. M. Robinson, G. E. Marti, D. G. Matei, T. Legero, M. Giunta, R. Holzwarth, F. Riehle, U. Sterr, and J. Ye, Demonstration of 4.8 times  $10^{-17}$  stability at 1s for two independent optical clocks, *Nature Photonics* **13**, 714 (2019).
- [22] S. M. Brewer, J.-S. Chen, A. M. Hankin, E. R. Clements, C. W. Chou, D. J. Wineland, D. B. Hume, and D. R. Leibbrandt,  $^{27}\text{Al}^+$  quantum-logic clock with a systematic uncertainty below  $10^{-18}$ , *Phys. Rev. Lett.* **123**, 033201 (2019).
- [23] S. Loriani, A. Friedrich, C. Ufrecht, F. D. Pumpo, S. Kleinert, S. Abend, N. Gaaloul, C. Meiners, C. Schubert, D. Tell, Étienne Wodey, M. Zych, W. Ertmer, A. Roura, D. Schlippert, W. P. Schleich, E. M. Rasel, and E. Giese, Interference of clocks: A quantum twin paradox, *Science Advances* **5**, eaax8966 (2019).
- [24] W. G. Unruh, Notes on black-hole evaporation, *Phys. Rev. D* **14**, 870 (1976).
- [25] L. C. B. Crispino, A. Higuchi, and G. E. A. Matsas, The Unruh effect and its applications, *Rev. Mod. Phys.* **80**, 787 (2008).
- [26] S. Takagi, Vacuum Noise and Stress Induced by Uniform Acceleration: Hawking-Unruh Effect in Rindler Manifold of Arbitrary Dimension, *Prog. Theor. Phys. Supp.* **88**, 1 (1986).
- [27] D. E. Bruschi, J. Louko, E. Martín-Martínez, A. Dragan, and I. Fuentes, Unruh effect in quantum information beyond the single-mode approximation, *Phys. Rev. A* **82**, 042332 (2010).
- [28] L. Sriramkumar and T. Padmanabhan, Finite-time response of inertial and uniformly accelerated unruh - de witt detectors, *Classical and Quantum Gravity* **13**, 2061 (1996).
- [29] W. Brenna, R. B. Mann, and E. Martín-Martínez, Anti-unruh phenomena, *Physics Letters B* **757**, 307 (2016).
- [30] L. J. Garay, E. Martín-Martínez, and J. de Ramón, Thermalization of particle detectors: The unruh effect and its reverse, *Physical Review D* **94**, 10.1103/physrevd.94.104048 (2016).
- [31] T. R. Perche and E. Martín-Martínez, Role of quantum degrees of freedom of relativistic fields in quantum information protocols, *Phys. Rev. A* **107**, 042612 (2023).
- [32] F. Dahia and P. J. F. d. Silva, Acceleration effects on atomic clocks, *Classical and Quantum Gravity* **32**, 177001 (2015).
- [33] S. Schlicht, Considerations on the Unruh effect: causality and regularization, *Class. Quantum Gravity* **21**, 4647 (2004).
- [34] J. Louko and A. Satz, How often does the Unruh-DeWitt detector click? regularization by a spatial profile, *Class. Quantum Gravity* **23**, 6321 (2006).
- [35] E. Martín-Martínez, T. R. Perche, and B. de S. L. Torres, General relativistic quantum optics: Finite-size particle detector models in curved spacetimes, *Phys. Rev. D* **101**, 045017 (2020).
- [36] E. Martín-Martínez and P. Rodriguez-Lopez, Relativistic quantum optics: The relativistic invariance of the light-matter interaction models, *Phys. Rev. D* **97**, 105026 (2018).
- [37] T. R. Perche, Localized nonrelativistic quantum systems in curved spacetimes: A general characterization of particle detector models, *Phys. Rev. D* **106**, 025018 (2022).
- [38] E. Poisson, The motion of point particles in curved spacetime, *Living Rev. Relativ.* **7**, 10.12942/lrr-2004-6 (2004).
- [39] E. Martín-Martínez, T. R. Perche, and B. d. S. L. Torres, Broken covariance of particle detector models in relativistic quantum information, *Phys. Rev. D* **103**, 025007 (2021).

- [40] W. G. Unruh and R. M. Wald, What happens when an accelerating observer detects a rindler particle, *Phys. Rev. D* **29**, 1047 (1984).
- [41] T. R. Perche, J. Polo-Gómez, B. d. S. L. Torres, and E. Martín-Martínez, Particle detectors from localized quantum field theories, *Phys. Rev. D* **109**, 045013 (2024).
- [42] A. M. Alhambra, A. Kempf, and E. Martín-Martínez, Casimir forces on atoms in optical cavities, *Phys. Rev. A* **89**, 033835 (2014).
- [43] A. Pozas-Kerstjens and E. Martín-Martínez, Entanglement harvesting from the electromagnetic vacuum with hydrogenlike atoms, *Phys. Rev. D* **94**, 064074 (2016).
- [44] R. Lopp and E. Martín-Martínez, Quantum delocalization, gauge, and quantum optics: Light-matter interaction in relativistic quantum information, *Phys. Rev. A* **103**, 013703 (2021).
- [45] R. Shah, E. Martín-Martínez, and T. R. Perche, Relativistic qft description for the interaction of a spin with a magnetic field, *Phys. Rev. D* **111**, 044075 (2025).
- [46] B. d. S. L. Torres, T. Rick Perche, A. G. S. Landulfo, and G. E. A. Matsas, Neutrino flavor oscillations without flavor states, *Phys. Rev. D* **102**, 093003 (2020).
- [47] T. R. Perche, C. Lima, and E. Martín-Martínez, Harvesting entanglement from complex scalar and fermionic fields with linearly coupled particle detectors, *Phys. Rev. D* **105**, 065016 (2022).
- [48] C. Gooding, S. Biermann, S. Erne, J. Louko, W. G. Unruh, J. Schmiedmayer, and S. Weinfurter, Interferometric Unruh detectors for bose-einstein condensates, *Phys. Rev. Lett.* **125**, 213603 (2020).
- [49] B. DeWitt, *General Relativity; an Einstein Centenary Survey* (Cambridge University Press, Cambridge, UK, 1980).
- [50] M. Good, B. A. Juárez-Aubry, D. Moustos, and M. Temir Khan, Unruh-like effects: effective temperatures along stationary worldlines, *J. High Energy Phys.* **2020** (6), 59.
- [51] K. Lorek, J. Louko, and A. Dragan, Ideal clocks—a convenient fiction, *Classical and Quantum Gravity* **32**, 175003 (2015).
- [52] S. Reinhardt, G. Saathoff, H. Buhr, L. A. Carlson, A. Wolf, D. Schwalm, S. Karpuk, C. Novotny, G. Huber, M. Zimmermann, *et al.*, Test of relativistic time dilation with fast optical atomic clocks at different velocities, *Nature Physics* **3**, 861 (2007).
- [53] B. Botermann, D. Bing, C. Geppert, G. Gwinner, T. W. Hänsch, G. Huber, S. Karpuk, A. Krieger, T. Kühl, W. Nörtershäuser, *et al.*, Test of time dilation using stored  $\text{Li}^+$  ions as clocks at relativistic speed, *Physical Review Letters* **113**, 120405 (2014).
- [54] P. Busch, The time-energy uncertainty relation, in *Time in quantum mechanics* (Springer, 2002) pp. 69–98.
- [55] D. Sen, The uncertainty relations in quantum mechanics, *Current Science*, 203 (2014).

## Appendix A: Explicit evaluation of the de-excitation probabilities for Alice and Bob

In this appendix, we present the expressions for the decay probability of Alice’s and Bob’s detectors that were used to obtain the results expressed in Figure 2.

First, for the sake of completeness, we recall that the decay probability of a smeared detector to leading order in the coupling strength is given by,

$$P = \lambda^2 \int dV dV' \Lambda(x) \Lambda(x') e^{i\Omega(\tau - \tau')} W(x, x'), \quad (\text{A1})$$

being  $\tau$  the time Fermi Normal coordinate [38] associated with the center of mass’s trajectory. Next, recall that the Minkowski vacuum function in 3 + 1 dimensions for a scalar, massless field admits the following plane wave expansion,

$$W(x, x') = \frac{1}{(2\pi)^3} \int \frac{d^3 \mathbf{k}}{2|\mathbf{k}|} e^{ik \cdot (x - x')}, \quad (\text{A2})$$

where  $\mathbf{k} = (|\mathbf{k}|, \mathbf{k})$  and  $\mathbf{k} \cdot x = \eta_{\mu\nu} x^\mu x^\nu$ , being  $\eta_{\mu\nu} = \text{diag}(-1, 1, 1, 1)$  the Minkowski metric. Defining the spacetime Fourier transform of the smearing as

$$\tilde{\Lambda}(|\mathbf{k}|, \mathbf{k}) := \int d^4 x \Lambda(x) e^{ik \cdot x}, \quad (\text{A3})$$

one can show that the de-excitation probability to leading order in perturbation can be written as

$$P = \frac{\lambda^2}{(2\pi)^3} \int \frac{d^3 \mathbf{k}}{2|\mathbf{k}|} |\tilde{\Lambda}(|\mathbf{k}| + \Omega, \mathbf{k})|^2. \quad (\text{A4})$$

Let us now adapt Eq. (A4) to the twin-paradox setup described in this paper. Working in inertial coordinates  $x = (t, \mathbf{x})$ , Alice’s clock (i.e., the detector’s center of mass) follows the  $\mathbf{z}_A(t) = (t, 0)$ , whereas Bob’s clock follows

$\mathbf{z}_B(\tau) = (t(\tau), x(\tau))$ , with the parametrization in function of the proper time  $\tau$  defined piecewise as follows ,

$$t(\tau) = \begin{cases} \frac{1}{a} \sinh(a\tau), & \tau \in (0, T/4), \\ \frac{1}{a} \sinh(a(\tau - T/2)) + \frac{2}{a} \sinh\left(\frac{aT}{4}\right), & \tau \in (T/4, 3T/4), \\ \frac{1}{a} \sinh(a(\tau - T)) + \frac{4}{a} \sinh\left(\frac{aT}{4}\right), & \tau \in (3T/4, T). \end{cases} \quad (\text{A5})$$

$$x(\tau) = \begin{cases} \frac{1}{a} \cosh(a\tau) - \frac{1}{a}, & \tau \in (0, T/4), \\ \frac{1}{a} \cosh(a(\tau - T/2)) + \frac{2}{a} \cosh\left(\frac{aT}{4}\right) - \frac{1}{a}, & \tau \in (T/4, 3T/4), \\ \frac{1}{a} \cosh(a(\tau - T)) - \frac{1}{a}, & \tau \in (3T/4, T). \end{cases} \quad (\text{A6})$$

From the expressions above we can also write the change from Alice's inertial coordinates  $(t, \mathbf{x}) = (t, x, y, z)$  to the Bob's Fermi normal coordinates  $(\tau, \boldsymbol{\xi}) = (\tau, X, y, z)$

$$t(\tau, X) = \begin{cases} \left(X + \frac{1}{a}\right) \sinh(a\tau), & \tau \in (0, T/4), \\ \left(-X + \frac{1}{a}\right) \sinh(a(\tau - T/2)) + \frac{2}{a} \sinh\left(\frac{aT}{4}\right), & \tau \in (T/4, 3T/4), \\ \left(X + \frac{1}{a}\right) \sinh(a(\tau - T)) + \frac{4}{a} \sinh\left(\frac{aT}{4}\right), & \tau \in (3T/4, T). \end{cases} \quad (\text{A7})$$

$$x(\tau, X) = \begin{cases} \left(X + \frac{1}{a}\right) \cosh(a\tau) - \frac{1}{a}, & \tau \in (0, T/4), \\ \left(X - \frac{1}{a}\right) \cosh(a(\tau - T/2)) + \frac{2}{a} \cosh\left(\frac{aT}{4}\right) - \frac{1}{a}, & \tau \in (T/4, 3T/4), \\ \left(X + \frac{1}{a}\right) \cosh(a(\tau - T)) - \frac{1}{a}, & \tau \in (3T/4, T). \end{cases} \quad (\text{A8})$$

Notice that the  $y$  and  $z$  coordinates remain unchanged due to Bob's motion being confined to the  $(t, x)$  plane.

The classical proper time associated with Alice's trajectory between events D and R is then

$$T_A = t(T) = \frac{4}{a} \sinh\left(\frac{aT}{4}\right). \quad (\text{A9})$$

For completeness, recall that Alice's clock is modelled using the smearing function

$$\Lambda_A(t, \mathbf{x}) = \mathbb{1}_{[0, T_A]}(t) F(\mathbf{x}), \quad (\text{A10})$$

with

$$F(\mathbf{x}) = \frac{e^{-(x^2+y^2+z^2)/2\sigma^2}}{(\sqrt{2\pi}\sigma)^3}, \quad (\text{A11})$$

The evaluation of Alice's decay probability,  $P_A$ , is then a straightforward application of Eq. (A4) using the smearing defined by Eq. (A10). After evaluating the Fourier transform of the smearing  $\Lambda_A$ , we write the integral in momentum space using spherical coordinates. The integral over the angular variables can be evaluated, leaving just one integral that needs to be evaluated numerically. The result is

$$P_A = \int_0^\infty d\omega \frac{e^{-\sigma^2\omega^2} \omega \sin^2\left(\frac{2(\omega-\Omega) \sinh(aT/4)}{a}\right)}{\pi^2 (\omega - \Omega)^2} = \frac{4 \sinh^2(aT/4)}{a^2} \int_0^\infty d\omega \frac{e^{-\sigma^2\omega^2} \omega \sin^2\left(\frac{2(\omega-\Omega) \sinh(aT/4)}{a}\right)}{4\pi^2 (\omega - \Omega)^2 \sinh^2(aT/4)/a^2} \quad (\text{A12})$$



$$= \frac{4 \sinh^2(aT/4)}{\pi^2 a^2} \int_0^\infty d\omega e^{-\sigma^2 \omega^2} \omega \operatorname{sinc}^2\left(\frac{2(\omega - \Omega) \sinh(aT/4)}{a}\right) \quad (\text{A13})$$

As for the evaluation of Bob's decay probability,  $P_B$ , first, we recall that the smearing to be used in this case is

$$\Lambda_B(\tau, \boldsymbol{\xi}) = \mathbb{1}_{[0, T_B]}(t) F(\boldsymbol{\xi}), \quad (\text{A14})$$

where  $T_B = T$  is the proper time associated with the trajectory  $\mathbf{z}_B$  between the events D and R, and  $(\tau, \boldsymbol{\xi}) = (\tau, X, y, z)$  are the Fermi normal coordinates built from Bob's worldline. Thus, defining  $\tilde{W}(\tau, X, y, z) = W(t(\tau, X), x(\tau, X), y, z)$ , we can write

$$P_B = \lambda^2 \int_0^T d\tau \int_0^T d\tau' \int dX dy dz dX' dy' dz' e^{i\Omega(\tau - \tau')} F(X, y, z) F(X', y', z') \tilde{W}(\tau, X, y, z), \quad (\text{A15})$$

where  $t(\tau, X)$  and  $x(\tau, X)$  are given by Eqs. (A7) and (A8), depending on the value of the parameter  $\tau$ , and the spatial profile  $F$  is given by Eq. (A11). To organize the integral of Eq. (A15) in a way that can be numerically solved, we explicitly substitute the expressions for  $F$ ,  $t(\tau, X)$  and  $x(\tau, X)$  for each range of the variable  $\tau$ , obtaining a total of nine integrals. Three of those integrals can be combined due to symmetries, leaving us with an expression of the form.

$$P_B = P_{11} + P_{22} + P_{33} + 2(\operatorname{Re}(P_{12}) + \operatorname{Re}(P_{13}) + \operatorname{Re}(P_{23})), \quad (\text{A16})$$

To write down an expression for each one of those terms, we use Eq. (A2) to write the plane wave expansion for the Wightman function, and then change to spherical coordinates when integrating over the momentum variables. At the end, we can write

$$P_{11} = \int_0^{T/4} d\tau \int_0^{T/4} d\tau' \int_0^\pi d\theta \int_0^\infty d\omega f_{11}(\tau, \tau', \theta, \omega), \quad (\text{A17})$$

$$P_{22} = \int_0^{T/4} d\tau \int_{3T/4}^T d\tau' \int_0^\pi d\theta \int_0^\infty d\omega f_{22}(\tau, \tau', \theta, \omega), \quad (\text{A18})$$

$$P_{33} = \int_{3T/4}^T d\tau \int_{3T/4}^T d\tau' \int_0^\pi d\theta \int_0^\infty d\omega f_{33}(\tau, \tau', \theta, \omega), \quad (\text{A19})$$

$$P_{12} = \int_0^{T/4} d\tau \int_{T/4}^{3T/4} d\tau' \int_0^\pi d\theta \int_0^\infty d\omega f_{12}(\tau, \tau', \theta, \omega), \quad (\text{A20})$$

$$P_{13} = \int_0^{T/4} d\tau \int_{3T/4}^T d\tau' \int_0^\pi d\theta \int_0^\infty d\omega f_{13}(\tau, \tau', \theta, \omega), \quad (\text{A21})$$

$$P_{23} = \int_{T/4}^{3T/4} d\tau \int_{T/4}^{3T/4} d\tau' \int_0^\pi d\theta \int_0^\infty d\omega f_{23}(\tau, \tau', \theta, \omega). \quad (\text{A22})$$

In the integrals above, the functions  $f_{ij}(\tau, \tau', \theta, \omega)$  can be explicitly written as

$$\begin{aligned}
f_{11}(\tau, \tau', \theta, \omega) = & \frac{1}{8\pi^2} \exp \left[ \frac{1}{8} \left( -\sigma^2 \omega^2 + 8i(\tau - \tau') \Omega + 3\sigma^2 \omega^2 \cos(2\theta) \right. \right. \\
& - \frac{\omega}{a} \left( -8i \cos \theta \cosh(a\tau) + 4a\sigma^2 \omega \cos^2 \theta \cosh^2(a\tau) + 8i(\cos \theta \cosh(a\tau') + \sinh(a\tau) - \sinh(a\tau')) \right. \\
& \left. \left. + a\sigma^2 \omega (2 \cosh(2a\tau) + (3 + \cos(2\theta)) \cosh(2a\tau') - 4 \cos \theta (\sinh(2a\tau) + \sinh(2a\tau'))) \right) \right] \omega \sin \theta,
\end{aligned} \tag{A23}$$

$$\begin{aligned}
f_{22}(\tau, \tau', \theta, \omega) = & \frac{1}{8\pi^2} \exp \left[ i(\tau - \tau') \Omega + \frac{\omega}{8a} \left( -8i \cos \theta \cosh\left(\frac{a}{2}(T - 2\tau)\right) \right. \right. \\
& + 8i \left( \cos \theta \cosh\left(\frac{a}{2}(T - 2\tau')\right) + \sinh\left(\frac{a}{2}(T - 2\tau)\right) - \sinh\left(\frac{a}{2}(T - 2\tau')\right) \right) \\
& - a\sigma^2 \omega \left( (3 + \cos 2\theta) \cosh(a(T - 2\tau)) + (3 + \cos 2\theta) \cosh(a(T - 2\tau')) \right. \\
& \left. \left. + 4 \sin^2 \theta - 4 \cos \theta (\sinh(a(T - 2\tau)) + \sinh(a(T - 2\tau'))) \right) \right) \right] \omega \sin \theta
\end{aligned} \tag{A24}$$

$$\begin{aligned}
f_{33}(\tau, \tau', \theta, \omega) = & \frac{1}{8\pi^2} \exp \left[ i(\tau - \tau') \Omega - \frac{\sigma^2 \omega^2}{8} \left( (3 + \cos 2\theta) \cosh(2a(T - \tau)) + (3 + \cos 2\theta) \cosh(2a(-T + \tau')) \right. \right. \\
& + 4(\sin^2 \theta + \cos \theta (\sinh(2a(T - \tau)) + \sinh(2a(T - \tau')))) \left. \right) \\
& + \frac{i\omega}{a} \left( \cos \theta (\cosh(a(-T + \tau)) - \cosh(a(-T + \tau'))) + \sinh(a(T - \tau)) + \sinh(a(-T + \tau')) \right) \left. \right] \omega \sin \theta
\end{aligned} \tag{A25}$$

$$\begin{aligned}
f_{12}(\tau, \tau', \theta, \omega) = & \frac{1}{8\pi^2} \exp \left[ \frac{1}{8} \left( -2\sigma^2 \omega^2 + 8i(\tau - \tau') \Omega + 2\sigma^2 \omega^2 \cos 2\theta \right. \right. \\
& + \frac{\omega}{a} \left( -a\sigma^2 \omega (3 + \cos 2\theta) [\cosh(2a\tau) + \cosh(a(T - 2\tau'))] \right. \\
& + 8i \left[ 2 \sinh\left(\frac{aT}{4}\right) - \sinh(a\tau) - \sinh\left(\frac{a}{2}(T - 2\tau')\right) \right] \\
& + 4 \cos \theta \left[ -4i \cosh\left(\frac{aT}{4}\right) + 2i \cosh(a\tau) + 2i \cosh\left(\frac{a}{2}(T - 2\tau')\right) \right. \\
& \left. \left. + a\sigma^2 \omega (\sinh(2a\tau) + \sinh(a(T - 2\tau'))) \right] \right) \left. \right] \omega \sin \theta
\end{aligned} \tag{A26}$$

$$\begin{aligned}
f_{13}(\tau, \tau', \theta, \omega) = & \frac{1}{8\pi^2} \exp \left[ \frac{1}{8} \left( -\sigma^2 \omega^2 + 8i(\tau - \tau') \Omega + 3\sigma^2 \omega^2 \cos 2\theta \right. \right. \\
& - \frac{\omega}{a} \left( -8i \cos \theta \cosh(a\tau) + 4a\sigma^2 \omega \cos^2 \theta \cosh^2(a\tau) \right. \\
& + 8i \left[ \cos \theta \cosh(a(-T + \tau')) - 4 \sinh\left(\frac{aT}{4}\right) + \sinh(a\tau) + \sinh(a(T - \tau')) \right] \\
& + a\sigma^2 \omega [2 \cosh(2a\tau) + (3 + \cos 2\theta) \cosh(2a(-T + \tau')) \\
& \left. \left. - 4 \cos \theta (\sinh(2a\tau) + \sinh(2a(-T + \tau')))] \right) \right] \omega \sin \theta
\end{aligned} \tag{A27}$$

$$\begin{aligned}
f_{23}(\tau, \tau', \theta, \omega) = & \frac{1}{8\pi^2} \exp \left[ \frac{1}{8} \left( -2\sigma^2\omega^2 + 8i(\tau - \tau')\Omega + 2\sigma^2\omega^2 \cos 2\theta \right. \right. \\
& + \frac{\omega}{a} \left( -a\sigma^2\omega(3 + \cos 2\theta) [\cosh(a(T - 2\tau)) + \cosh(2a(-T + \tau'))] \right. \\
& + 8i \left[ 2 \sinh\left(\frac{aT}{4}\right) + \sinh\left(\frac{a}{2}(T - 2\tau)\right) + \sinh(a(-T + \tau')) \right] \\
& + 4 \cos \theta \left[ 4i \cosh\left(\frac{aT}{4}\right) - 2i \cosh\left(\frac{a}{2}(T - 2\tau)\right) - 2i \cosh(a(-T + \tau')) \right. \\
& \left. \left. \left. + a\sigma^2\omega (\sinh(a(T - 2\tau)) + \sinh(2a(-T + \tau'))) \right] \right) \right] \omega \sin \theta
\end{aligned} \tag{A28}$$

### Appendix B: Inertial clocks

In this appendix, we analyze the behaviour of our clock for the case of an inertial trajectory. Using the same spatial profile as in Eq.(5), we will explicitly show that, in the limit where the clock's size is negligible compared to the measured times, our model matches the predictions of an ideal clock.

Concretely, when the system that composes the clock undergoes an inertial trajectory in Minkowski spacetime and interacts with the field for a proper time  $T$  following the switching model  $\chi(t) = \mathbb{1}_{[0, T]}(t)$ , we have

$$P(T) = \left( \frac{T}{2\pi} \right)^2 \int_0^\infty d\omega e^{-\sigma^2\omega^2} \omega \operatorname{sinc}^2\left(\frac{(\omega - \Omega)T}{2}\right). \tag{B1}$$

Now, by defining the variable  $u = \omega/T$ , and then performing a translation  $u \rightarrow u + \Omega T$ , we can write

$$\begin{aligned}
P(T) &= \frac{1}{(2\pi)^2} \int_0^\infty du e^{-\sigma^2 u^2 / T^2} u \operatorname{sinc}^2\left(\frac{(u - \Omega T)}{2}\right), \\
&= \frac{1}{(2\pi)^2} \int_{-\Omega T}^\infty du e^{-\sigma^2 (u + \Omega T)^2 / T^2} (u + \Omega T) \operatorname{sinc}^2\left(\frac{u}{2}\right)
\end{aligned} \tag{B2}$$

Thus, the average de-excitation write can be cast as

$$\frac{P(T)}{T} = \frac{1}{(2\pi)^2} \int_{-\Omega T}^\infty du e^{-\sigma^2 (u/T + \Omega)^2} \left(\frac{u}{T} + \Omega\right) \operatorname{sinc}^2\left(\frac{u}{2}\right). \tag{B3}$$

Now, we would like to evaluate the limit of the expression above when  $T \rightarrow \infty$ , which corresponds to the scenario where the effective clock's size, as measured by  $\sigma$ , is negligible compared to the times measured by this clock. We have

$$\begin{aligned}
\lim_{T \rightarrow \infty} \frac{P(T)}{T} &= \lim_{T \rightarrow \infty} \frac{1}{(2\pi)^2} \int_{-\infty}^\infty du e^{-\sigma^2 (u/T + \Omega)^2} \left(\frac{u}{T} + \Omega\right) \operatorname{sinc}^2\left(\frac{u}{2}\right) \\
&= \lim_{T \rightarrow \infty} \frac{1}{(2\pi)^2} \left( \Omega \int_{-\infty}^\infty du e^{-\sigma^2 (u/T + \Omega)^2} \operatorname{sinc}^2\left(\frac{u}{2}\right) + \frac{1}{T} \int_{-\infty}^\infty du e^{-\sigma^2 (u/T + \Omega)^2} u \operatorname{sinc}^2\left(\frac{u}{2}\right) \right) \\
&= \lim_{T \rightarrow \infty} \frac{\Omega}{(2\pi)^2} \int_{-\infty}^\infty du e^{-\sigma^2 (u/T + \Omega)^2} \operatorname{sinc}^2\left(\frac{u}{2}\right) \\
&= \frac{\Omega}{(2\pi)^2} \int_{-\infty}^\infty du \lim_{T \rightarrow \infty} \left( e^{-\sigma^2 (u/T + \Omega)^2} \right) \operatorname{sinc}^2\left(\frac{u}{2}\right) \\
&= \frac{\Omega e^{-\sigma^2 \Omega^2}}{(2\pi)^2} \int_{-\infty}^\infty du \operatorname{sinc}^2(u/2) \\
&= \frac{\Omega e^{-\sigma^2 \Omega^2}}{2\pi},
\end{aligned} \tag{B4}$$

where we can commute the limit with the integral using the dominated convergence theorem due to the fact that

$e^{-\sigma^2(u/T+\Omega)^2} \text{sinc}^2(u/2) \leq e^{-\sigma^2\Omega^2} \text{sinc}^2(u/2)$ . Notice that this result is only valid for  $\sigma > 0$ , and the de-excitation probability diverges in the limit  $\sigma \rightarrow 0$  (see Eq. (B1)). That is, the limits  $T \rightarrow \infty$  and  $\sigma \rightarrow 0$  do not commute. Therefore, by Eq.(B4), we have proven that in the limit  $T \rightarrow \infty$ , our clock behaves exactly as an ideal clock, with the proportionality constant between the decay probability and the time measured given by

$$\alpha_\infty = \frac{\Omega e^{-\sigma^2\Omega^2}}{2\pi}. \quad (\text{B5})$$

Now, if one wishes to use this same clock to measure a finite time  $T$ , the relative deviation from the ideal case will be

$$\alpha(T, \Omega, \sigma) \equiv \frac{|P(T)/T - \alpha_\infty|}{\alpha_\infty}. \quad (\text{B6})$$

In Figure 3, we display the values of the relative deviation  $\alpha(T, \Omega, \sigma)$  for different clocks' sizes with energy gap  $\Omega = 2T_0$ , for some fixed timescale  $T_0$ . We observe that, when the clock's size is about  $10^3$  smaller than the times being measured, the relative error compared to the ideal clock is less than 0.3%. For the case used to explore the twin paradox scenario, Alice's clock is at most of size  $\sigma = 0.3T_0$  and for  $T = 10T_0$ , the deviation from the standard clock constant is at most 5%, being 1% for the smallest clock size considered of  $\sigma = 0.1T_0$ .

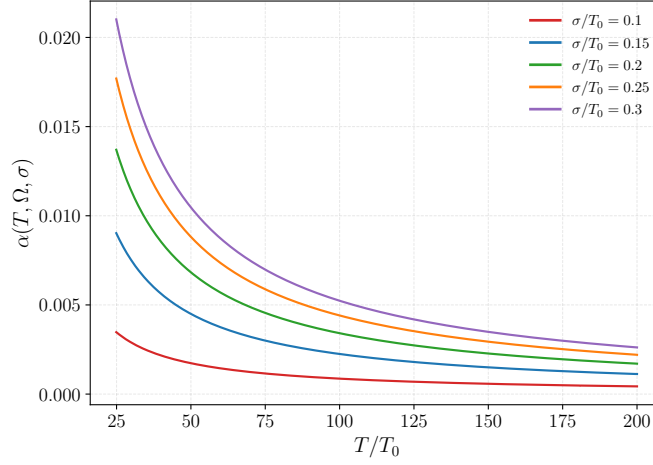


Figure 3. Relative deviation  $\alpha(T, \Omega, \sigma)$  between our model and an ideal clock in an inertial scenario, for different clock sizes (as controlled by the parameter  $\sigma$ ) and with energy gap  $\Omega = 2T_0$ .